Available online at www.sciencedirect.com

ScienceDirect

Journal of Membrane Science 298 (2007) 71–79

journal of MEMBRANE SCIENCE

www.elsevier.com/locate/memsci

Nanocomposite MFI-alumina membranes via pore-plugging synthesis: Specific transport and separation properties

S. Miachon[a,*], P. Ciavarella[a], L. van Dyk[a], I. Kumakiri[a], K. Fiaty[b], Y. Schuurman[a], J.-A. Dalmon[a]

[a] *Institut de Recherches sur la Catalyse et l'Environnement de Lyon (IRCELYON), UMR5256 CNRS, Université Claude Bernard Lyon 1, 2, av. A. Einstein, 69626 Villeurbanne Cedex, France*

[b] *Laboratoire d'Automatique et de Génie des Procédés (LAGEP), UMR5007 CNRS, Université Claude Bernard Lyon 1, 43, bd. du 11 Novembre 1918, 69622 Villeurbanne Cedex, France*

Received 13 February 2007; received in revised form 28 March 2007; accepted 3 April 2007

Abstract

Nanocomposite MFI-alumina membranes, obtained by growing zeolite crystals within the porosity of a host macroporous support (pore-plugging method), as described in a previous paper, were studied for their behaviour for pure gas permeation and gas mixture separation. Hydrogen, nitrogen and light hydrocarbons were permeated on a wide range of temperatures, up to 873 K for hydrogen. All pure gases results are well described by the generalised Maxwell–Stefan equation, with no need for an additional "activated gas transport" term, as no flux increase was observed at higher temperatures. Two examples of gas separations were carried out up to 723 K (*n*-butane/hydrogen) and 673 K (xylene isomers) that similarly show regular flux decreases at higher temperatures.

These results were compared to literature data on film-like MFI zeolite membranes that generally show a flux increase at high temperature. This discrepancy was attributed to the reversible opening of intercrystalline pathways in film-like membranes upon heating. These openings were computed, taking benefit of recently published zeolite thermal expansion data, and their contribution to the permeation was evaluated.

Keywords: Zeolite membrane; Nanocomposite; Gas separation; Thermal expansion; Xylenes; Hydrogen; Nitrogen; Light hydrocarbons

1. Introduction

For more than a decade, many works have been reported on zeolite membranes, as described in several reviews [1–9]. In particular, gas transport through zeolite membranes has been attracting a lot of attention [1,3–8,10–20]. These membranes typically present a zeolite film structure on top of a porous support and some authors have insisted on this aspect [21–24].

Generally, the membrane permeance does not follow an adsorption-only driven mechanism, as the transmembrane flux, after going through a maximum, in keeping with adsorption, increases again at higher temperatures [2,12]. For instance, Kapteijn's group reported this behaviour for light hydrocarbons, using a film-like zeolite (silicalite 1) layer on top of a porous stainless steel support [12,25,26]. Noble and Falconer [11] described a similar curve shape for a silicalite membrane on porous alumina. Matsukata and co-workers [27], using MFI on porous alumina, also showed a sharp increase of isobutene flux above 673 K.

In the case of gas mixture separation, Kapteijn's group previously published data for butane/hydrogen mixtures [15], showing an increase of both gas fluxes above 500 K. More recently, Tarditi et al. [28] published xylene isomer separation results, through silicalite (*c*-axis oriented) membranes on porous stainless steel supports. A sharp flux increase was observed for *ortho* and *meta*-xylene above 500 K, and for *para*-xylene above 573 K.

To face the complication of an increasing flux at high temperatures, a few authors have introduced a "gas activated transport" [26,29] on top of the Langmuir-coverage based model of diffusion, also known as generalised Stefan–Maxwell.

At variance to some authors insisting on the advantages of film-like structure [24,30], we have been working on a different approach: the zeolite/alumina nanocomposite membrane, where

---

[*] Corresponding author. Tel.: +33 472445384.
E-mail address: sylvain.miachon@ircelyon.univ-lyon1.fr (S. Miachon).

0376-7388/$ – see front matter © 2007 Elsevier B.V. All rights reserved.
doi:10.1016/j.memsci.2007.04.008

the separative layer is made of zeolite material grown inside the porosity of an alumina support. The preparation of this type of membrane [31], its permeance and separation properties [32,33], quality testing [34] and applications to catalytic membrane reactors [35–37] have been previously published. First results of permeation [32] showed a behaviour different from that reported in the literature: at high temperature, the composite membrane did not show the flux increase generally observed.

Very recently, we published a detailed description of the preparation and structural properties of the composite membrane [38]. Among other characterisation results, a thorough transmission electronic micrographs suggested that zeolite crystal grain boundaries should not participate in the permeation across the membrane. Indeed, the same zeolite crystal, plugging neighbouring support pores, was observed, without crystal boundaries. These specific features prompted us to study more in detail gas transport through this particular type of material.

Here we show the temperature dependence of permeation through the nanocomposite membrane for a series of gases is different from that reported in film-like membranes. This observation will be related to the nanocomposite architecture.

2. Experimental

2.1. Material and gases

MFI zeolite membranes were prepared using alumina asymmetric porous tubular support (made of three layers with pores of 12 μm–0.8 μm–0.2 μm successively) provided by Pall-Exekia (T1-70 type). These supports were 15 cm long, 1 cm diameter, and included 1.5 cm enamel endings for sealing purposes. Interrupted hydrothermal synthesis was carried out, using a 3-day aged precursor solution of 1 SiO_2:0.45 TPAOH:27.8 H_2O molar proportions. Template removal was achieved by calcination in air at 500 °C. A detailed study of this preparation can be found in a previous paper [38].

2.2. Gas transport

2.2.1. Set-up

Tubular membranes were mounted in a graphite-sealed test module, showed in Fig. 1. Before any gas transport measurement, the membrane was first treated at 400 °C under both-side 20 ml/min flow of nitrogen for 6 h, to remove adsorbed species, such as water coming from air humidity when the sample is exposed to atmosphere.

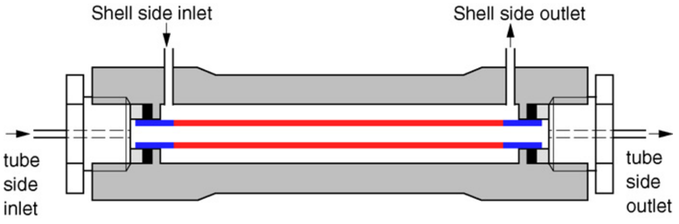

Fig. 1. Schematic drawing of the permeation test module, showing the tubular membrane and graphite sealing.

Single gas permeance for hydrogen, helium, nitrogen and hydrocarbons were carried out with a feed pressure slightly over 100 kPa, a pressure difference close to 10 kPa. A regulating valve at the outlet of the retentate compartment was used to adjust the internal pressure. Another regulating valve at the outlet of the permeate controlled the transmembrane pressure difference. More details can be found in previous papers [33].

The temperature was varied in steady state steps from 293 to 723 K, and up to 860 K in one case (hydrogen).

2.2.2. Gas mixture separation

Gas separation was carried out on *n*-butane/hydrogen and xylene isomer mixtures, using modified Wicke-Kallenbach protocols. Stream composition was analysed using a Shimadzu GC 14A gas chromatograph equipped with a 0.19% picric acid/graphpack GC column with an FID detector (*n*-butane), a carbosphere column with a TCD detectors (hydrogen) and a Solgel-WAX capillary column with an FID detector (xylenes).

N-Butane/hydrogen separation was carried out with the same feed (hydrogen:*n*-butane:nitrogen = 12:15:73) and sweep (nitrogen) flow rates (54 μmol/s), close to atmospheric pressure. The temperature was increased from 300 to 723 K in 10 steps, waiting sufficient time for equilibrium.

For xylene separation, a mixture of isomers (1.5 kPa *p*-xylene, 4.5 kPa *m*-xylene and 1.35 kPa *o*-xylene) saturated in nitrogen at atmospheric pressure and 336 K was fed at 60 ml/min with a counter-current nitrogen sweep of 15 ml/min. The temperature of the membrane system was varied from 673 to 423 K and again from 423 to 673 K in six steps. In this case as well, all measurements were taken at steady state.

2.2.3. Model of pure gas permeation

All results of pure gas permeation were fitted using a model based only on the Stefan–Maxwell approach, that takes into account exclusively adsorption phenomena [39,40]. This lead to the following variation of flux:

$$J = \frac{c_{\mathrm{sat}}\rho\varepsilon D_0^{\infty}}{\tau L}\ln \times \left[\frac{1+(p_{\mathrm{R}}/p^0)\exp((\Delta S^{\circ}_{\mathrm{ads}}/R)-(\Delta H^{\circ}_{\mathrm{ads}}/RT))}{1+(p_{\mathrm{P}}/p^0)\exp((\Delta S^{\circ}_{\mathrm{ads}}/R)-(\Delta H^{\circ}_{\mathrm{ads}}/RT))}\right] \times \exp[-E_{\mathrm{D}}/RT] \tag{1}$$

with R: ideal gas constant (8.314 J/mol/K), c_{sat}: concentration of the gas at saturation in the MFI crystals (mol/kg), ρ_{MFI}: density of the MFI (1700 kg/m^3), ε: porosity of the material (0.075), obtained by the product of support and MFI porosity values, D_0^{∞}: Stefan–Maxwell diffusivity (m^2/s, fitted parameter), τ: tortuosity (1.2), as indicated by the support provider, L: membrane equivalent thickness (3×10^{-6} m), p_{R}: retentate pressure (Pa), p_{P}: permeate pressure (Pa), p^0: reference atmospheric pressure (101,325 Pa), $\Delta S^{\circ}_{\mathrm{ads}}$: adsorption entropy (J/mol/K), $\Delta H^{\circ}_{\mathrm{ads}}$: adsorption enthalpy (J/mol), and E_{D}: diffusion activation energy (J/mol, fitted parameter).

The membrane effective thickness ($L = 3$ μm) was obtained by comparing different gas permeances at a fixed tempera-

Table 1
Parameters used and *fitted* in Stefan–Maxwell Eq. (1)

Gas	Experimental		Fixed adsorption parameters			*Fitted parameters*	
	P_R (kPa)	P_P (kPa)	c_{sat} (mol/kg)	ΔS°_{ads} (J/mol/K)	ΔH°_{ads} (kJ/mol)	D_0^∞ (10^{-8} m²/s)	E_D (kJ/mol)
H_2	120	112.4	5.4	−43.0	−5.9	1.8	2.0
N_2	128	112.5	5.4	−50.0	−13.8	0.4	4.0
CH_4	130	107	2.2	−68.5	−19.0	31	9.4
C_2H_6	130	107	1.9	−75.4	−30.5	6.1	8.8
C_3H_8	130	104	1.5	−77.3	−36.4	3.0	9.7
C_4H_{10}	131	103	1.4	−85.9	−44.6	2.0	11.8

The adsorption parameters are from literature (c_{sat} [43], entropy and enthalpy for H_2 and N_2 [26] and present work for hydrocarbons.

ture, using Eq. (1), and taking into account various diffusivity data.

Adsorption data (ΔS°_{ads} and ΔH°_{ads}) were obtained from literature in the case of hydrogen and nitrogen [26]. For hydrocarbons, they were measured in a TAP reactor [41]. To get data on the very material used in this work, 1 cm of the crushed and sieved membrane, containing 1.5 wt% of zeolite, was sandwiched between two layers of quartz particles in the reactor. Before the pulse experiments the reactor was heated to 673 K under a nitrogen flow to desorb any adsorbed water. After this pre-treatment the reactor was evacuated. The different hydrocarbons were mixed with 10% argon. Pulse experiments were conducted at temperatures between 373 and 493 K. The modelling of the pulse responses to extract the sorption parameters is described in detail in [42]. The entropy of adsorption was calculated by assuming 8 sites per unit cell [43]. All sorption parameters are reported in Table 1.

3. Results

3.1. Single gas transport

Fig. 2 (top) shows a typical flux variation of hydrogen and nitrogen through nanocomposite alumina/zeolite membranes, as a function of temperature. Several samples were used to obtain this data, providing similar results. Eq. (1) is fitted to the data in each case. Table 1 gives the test conditions and the fitting parameters for these temperature variations. Hydrogen and nitrogen show a continuous decrease of flux with temperature. Fitted Stefan–Maxwell curves indicate a flux maximum located at a higher temperature for nitrogen than hydrogen.

The bottom of the same figure and the four last rows of Table 1 show corresponding results for hydrocarbons (methane to *n*-butane). The above mentioned flux maximum can also be seen in these cases, with a temperature increasing with the length of the hydrocarbon chain, as is commonly expected.

Please note the observed variations show no indication of flux increase at higher temperature, up to 720 K for the six gases tested here. In all cases, the fitted parameters are consistent with commonly accepted values [26,44].

In order to check this monotonous decreasing trend, an experiment at higher temperature was carried out on another membrane. The flux variation is shown in Fig. 3, together with a fitted curve following the Stefan–Maxwell model (with similar parameters). It can clearly be seen than no flux increase appears, even up to 860 K. The low-temperature flux values of this sample, as measured after this treatment, were not affected. This shows the integrity of the nanocomposite membrane material when used for significant periods of time in such hard conditions.

3.2. Gas separation

Fig. 4 shows a typical result of hydrogen/*n*-butane mixture separation. The transmembrane flux of both gases is shown as a

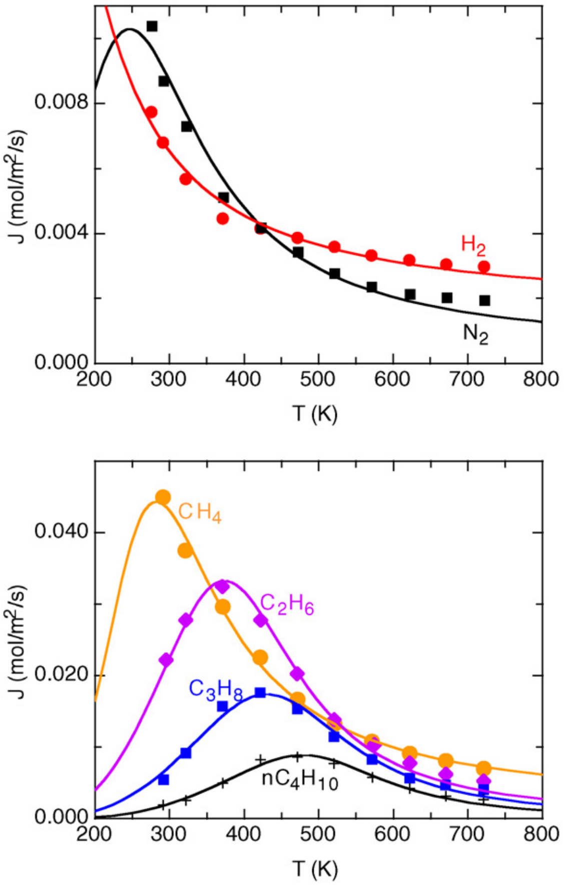

Fig. 2. Single gas permeance variations of hydrogen (●), nitrogen (■) (top) and of four hydrocarbons (bottom): methane (●), propane (♦), ethane (■) and normal butane (+) through nanocomposite MFI/alumina membranes. Points: experimental data, curves: Stefan–Maxwell Eq. (1) fitted to the data points (Table 1 gives the fixed and fitted parameters).

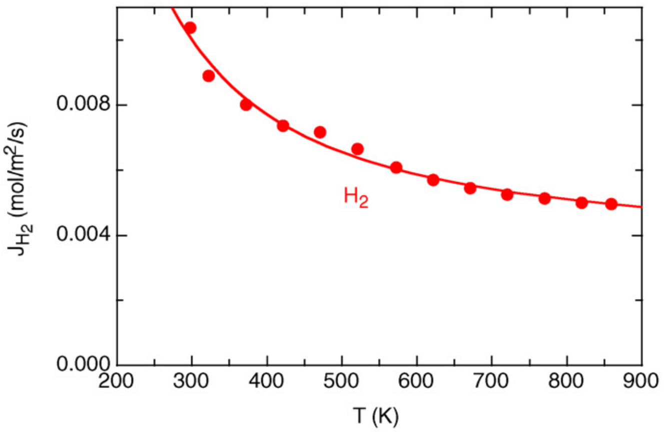

Fig. 3. Single gas flux variation of hydrogen through an MFI/alumina nanocomposite membrane on a larger temperature range (similar exp. conditions than in Table 1). Points: experimental data, curve: Stefan–Maxwell Eq. (1) fitted to the data points.

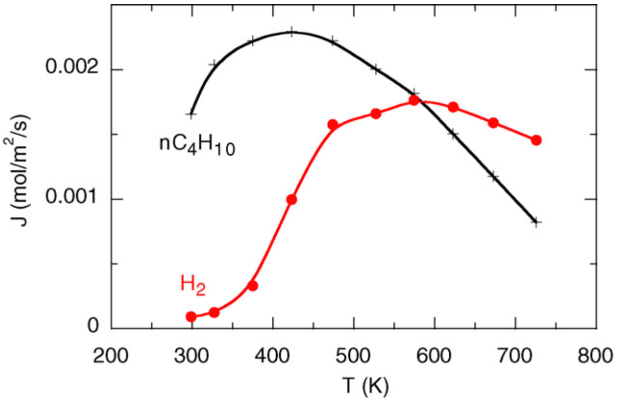

Fig. 4. Gas flux of hydrogen (●) and normal butane (+) in an equimolar mixture diluted in nitrogen (Wicke-Kallenbach mode), through an MFI/alumina nanocomposite membrane. Lines are guides to the eye.

function of temperature, from 300 to 723 K. For both gases, the permeance shows a decrease at higher temperatures.

Fig. 5 shows another example of gas separation on the same type of membrane. *Para*-xylene is selectively separated from a mixture of isomers diluted in nitrogen, in the 400–700 K temperature range. Once again, the transmembrane flux of the only detected isomer regularly decreases at higher temperatures. The other isomers can be neglected in the transport model. They are too bulky to penetrate the zeolite pores (true molecular sieving). For that reason, the pure-gas Stefan–Maxwell model used previously can be applied. The fitting provides data of diffusivity and activation energy ($\approx 10^{-11}$ m^2/s and 14 kJ/mol, respectively). It has to be noted that no increase of other isomer transmembrane flux was observed at higher temperatures, maintaining an apparent infinite selectivity of the membrane towards *p*-xylene.

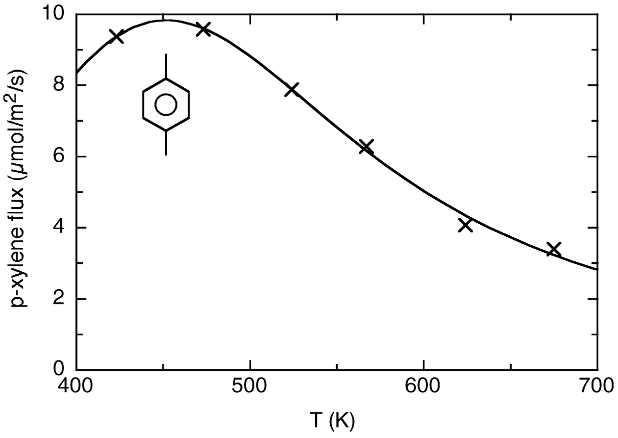

Fig. 5. Separation of *para*-xylene through an MFI/alumina nanocomposite membrane (from a mixture of isomers diluted in nitrogen). Only *para*-xylene is detected. Points: experimental data, curve: Stefan–Maxwell Eq. (1) fitted to the data points (taking into account *para*-xylene only).

4. Discussion

4.1. Single gas transport

The absolute permeance values obtained in this work are in same order of magnitude than that of the literature, consistently with another study on intrapore synthesised zeolite membranes [45]. Contrarily, in some papers [24,30], it is mentioned that embedding the crystals into the support pores may lead to smaller permeance values. The idea is that the geometric surface area of the membrane is reduced to that of the support pore openings. This can be debated, as in film-like membranes the toplayer is in contact with the support, and therefore the available surface area, on the support side, is reduced in the same way.

As mentioned in the introduction, in the last 10 years, many scientific papers have reported high temperature gas flux increase through MFI zeolite membranes. About all works report a permeance variation including a minimum following a maximum, provided their experimental temperature ranges high enough. Table 2 (single gas) and Table 3 (mixtures) gives an overview of this aspect from a series of papers, illustrating the maximum (at T_B) and minimum (at T_C) of the corresponding curve (Fig. 6).

In Fig. 2, the maxima (T_B) observed here are: H_2: <200 K, N_2: 250 K, CH_4: 280 K, C_2H_6: 370 K, C_3H_8: 420 K, *n*-C_4H_{10}: 470 K. These values are consistent with literature data summarized in Table 2.

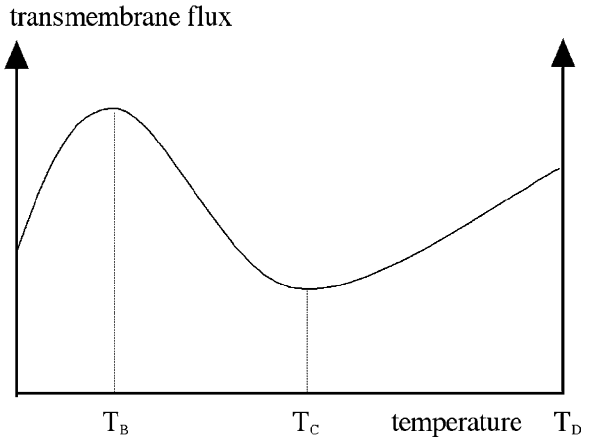

Fig. 6. Typical transmembrane flux temperature through MFI membranes as reported in literature. T_D represents the maximum temperature used for testing.

Table 2
Summary of the pure gas permeance-temperature dependence observed through MFI membranes in the literature (SS: stainless steel, T_A, T_B and T_C refer to temperature points illustrated in Fig. 7)

Gas	Membrane	Cryst. size (μm)	Support	Pore size	T_B (K) maximum	T_C (K) minimum	T_D (K) limit	Reference	Note
H_2	Silicalite-1	–	γ-Al_2O_3	5 nm	<293	350	600	[14]	
	ZSM5	5–10 μm	γ-Al_2O_3	5 nm	<293	380	550	[20]	
	ZSM5	2 μm	α-Al_2O_3	0.2 μm	<293	<293	550	[20]	
	HZSM5 Si/Al = 600	–	Al_2O_3	–	<300	375	530	[60]	
	HZSM5 Si/Al = 600	–	SS	–	<300	350	530	[60]	
	HZSM5 Si/Al = 25	–	SS	0.5 μm	<320	<320	523	[61]	
	HZSM5 Si/Al = 600	–	SS	0.5 μm	<320	460	–	[61]	
	Silicalite	0.5 μm	α-Al_2O_3	0.2 μm	<300	<300	420	[62]	Undesorbed mat.
N_2	HZSM5 Si/Al = 600	–	Al_2O_3 or SS	–	<300	475	530	[60]	
	HZSM5 Si/Al = 25	–	SS	0.5 μm	<320	>523	–	[61]	
CH_4	Silicalite-1	–	SS	–	240	480	673	[25]	
	Silicalite	0.5 μm	α-Al_2O_3	0.2 μm	<300	<300	420	[62]	Undesorbed mat.
	Silicalite	0.5 μm	α-Al_2O_3	0.2 μm	<300	<300	420	[62]	Undesorbed mat.
	ZSM5	–	SS	–	<300	>500	500	[63]	Transient exp.
	ZSM5	–	SS	–	<300	500	773	[19]	Transient exp.
C_2	Silicalite-1	–	SS	–	350	570	673	[25]	
	ZSM5	–	SS	–	370	500	773	[19]	Transient exp.
C_3	Silicalite-1	–	SS	–	400	580	620	[12]	
	ZSM5	–	SS	–	430	>500	500	[63]	Transient exp.
	ZSM5	–	SS	–	440	>500	500	[19]	Transient exp.
	MFI	~5 μm	α-Al_2O_3	0.2 μm	410	580	773	[64]	
nC_4	Silicalite-1	–	SS	–	430	620	620	[12]	
	Silicalite-1	–	γ-Al_2O_3	5 nm	–	–	600	[14]	
	ZSM5	2 μm	α-Al_2O_3	0.2 μm	<293	>550	–	[20]	
	HZSM5 Si/Al = 25	–	SS	0.5 μm	480	>523	–	[61]	
	HZSM5 Si/Al = 600	–	SS	0.5 μm	460	>523	–	[61]	
	ZSM5	–	SS	–	460	>500	500	[63]	Transient exp.
	ZSM5	–	SS	–	460	500	773	[19]	Transient exp.

As for the minimum (T_C), the values reported in other works are less consistent than for T_B values. However, it is clear that the behaviour of the nanocomposite membrane is quite different from what is observed in literature: here, a continuous flux decrease is always present at higher temperatures. Let us now consider the possible reasons of such a difference.

Apart from their distinctive nanocomposite structure, the membrane materials reported here differ from most of the materials presented in literature in terms of acidity. As shown in a previous work [38], the silicon/aluminium ratio is very low, close to 10. This makes it one of the lowest Si/Al MFI material reported, even in powder form. These many acidic sites are very strong adsorption sites, and may account for a large part in the adsorption-driven mechanism of transmembrane gas transport [46]. However, this Si/Al ratio data is almost never available in literature reports dealing with high-temperature gas transports in zeolite membranes. Moreover, if one makes the hypothesis that this particularly high acidity of the nanocomposite mem-

Table 3
Summary of the gas mixture flux-temperature dependence observed through MFI membranes in the literature (SS: stainless steel, T_A, T_B and T_C refer to temperature points illustrated in Fig. 7)

Mixture (gas)	Membrane	Cryst. size (μm)	Support	Pore size	T_B (K) maximum	T_C (K) minimum	T_D (K) limit	Reference
$nC_4 + H_2$ (H_2)	Silicalite-1	–	SS	–	–	400	620	[12]
Xylenes (*p*-xylene)	Silicalite-1	–	SS	0.5 μm	420	460	490	[65]
	HZSM5	–	SS	0.5 μm	440	480	530	[65]
	BZSM5	–	SS	0.5 μm	<400	480	510	[65]
	ZSM5, c-oriented	2–3 μm	α-Al_2O_3	0.2 μm	400	470?	473	[66]
	ZSM5, hoh oriented	2–3 μm	α-Al_2O_3	0.2 μm	400	–	473	[66]
	Silicalite-1	≈15 μm	SS	0.2 μm	<323	573	673	[28]
	HZSM5	>15 μm	SS	0.2 μm	–	–	673	[28]
	Silicalite-1, a-oriented	<0.2 μm	α-Al_2O_3	0.1 μm	≈300	–	650	[30]
	MFI, b-oriented	0.1–0.5 μm	SiO_2	2 nm	400	–	500	[67]
	MFI	0.5 μm	α-Al_2O_3	0.2 μm	520	573	623	[68]

branes could be the reason for a high-temperature shift of the curve minimum (T_C), it is quite unlikely that this point could reach a temperature higher than 860 K for such a low adsorbing species as hydrogen (Fig. 3).

Another hypothesis could be related to intercrystalline pathways. The contribution of grains boundaries to transport properties has been discussed in various studies. The number and size of these boundaries has been considered in a comparison of a range of membranes [20] in order to explain some differences in their behaviour. Nevertheless, all samples described in that study show a permeance increase at higher temperature. Recently, Nakao's group provided a full study of ground boundary influence on the gas permeation through this type of defects in zeolite membranes [47], following an interesting work of Au and Yeung on the relation between the zeolite film structure and its transport properties [48]. Some works have been published on the effect of temperature on the opening of intercrystalline pores, or even cracks, during membrane calcination [49–51]. However, to our best knowledge, no study was published that takes benefit from the recent data obtained on the MFI thermal behaviour. Let us consider this option in details.

4.2. Thermal behaviour of the membranes

Recently, several works have been published on the thermal behaviour of zeolites. Yamahara et al. [52], using molecular dynamics calculations, predicted a thermal contraction behaviour of MFI-type zeolites above 400 K (orthorhombic/HT-orthorombic transition), with a difference according to the cell direction. Park et al. [53], using the Guinier XRD technique, were able to obtain first measurements supporting the above. Later on, Marinkovic et al. [54], obtained more accurate data on hydrated HZSM-5, using Rietveld high-resolution synchrotron XRD. Very recently, Bhange and Ramaswamy [55] published a detailed study of silicalite-1 and Zr-silicalite-1 using the same technique, this time on dry material, showing this contraction effect is not only related to water departure. Finally, in a similar approach, Dalconi et al. [56] published an extensive study of Cu-ZSM5 crystal parameter size evolution from room temperature to 1200 K, in keeping with Bhange's results. Besides the transition from monoclinic to orthorhombic phases at about 400 K, they showed that the contraction of the crystals depends on the crystallographic direction. Lattice parameters *a* reduces linearly by about 0.32% over the 700 K range, whereas *c* contraction is 0.25% and *b* 0.20% over the same temperature range. The latter only decreases above 670 K.

The origin of this specific thermal behaviour is discussed by Bhange and Ramaswamy [55]. The departure of water molecules is often accounted for this phenomenon. However, they show that beyond this aspect, the Si–O–Si bond angle variation is the actual reason for the reversible thermal behaviour.

In the present work, a simple geometric model was set-up, in order to consider the influence on transport properties of intercrystalline pore thermal opening for zeolite films deposited on porous supports. All the above data are in agreement. Considering the type of material used in the membranes of the literature, the data of Bhange and Ramaswamy [55] appear the most convenient. In this approach, homogeneously sized crystals of MFI material, connected together but without adherence between each other are considered on the support. Knowing the size of the crystallites, the thermal expansion of the alumina ($8.5 \times 10^{-6}\ K^{-1}$) and the crystallographic parameter values of the MFI as a function of temperature, it is straightforward to devise the resulting evolution of intercrystalline space. Fig. 7 shows the results of these calculations. Part (b) describes, for a crystal size of 1 μm, the intercrystalline pore opening as a function of the crystallographic direction, as well as the value calculated for a non-oriented system (i.e. as obtained from the unit cell volume). Fig. 7(a) shows the non-oriented case, with different crystal sizes. Similar results can be computed with stainless steel as a support, leading to even larger values, due to its larger thermal expansion coefficient.

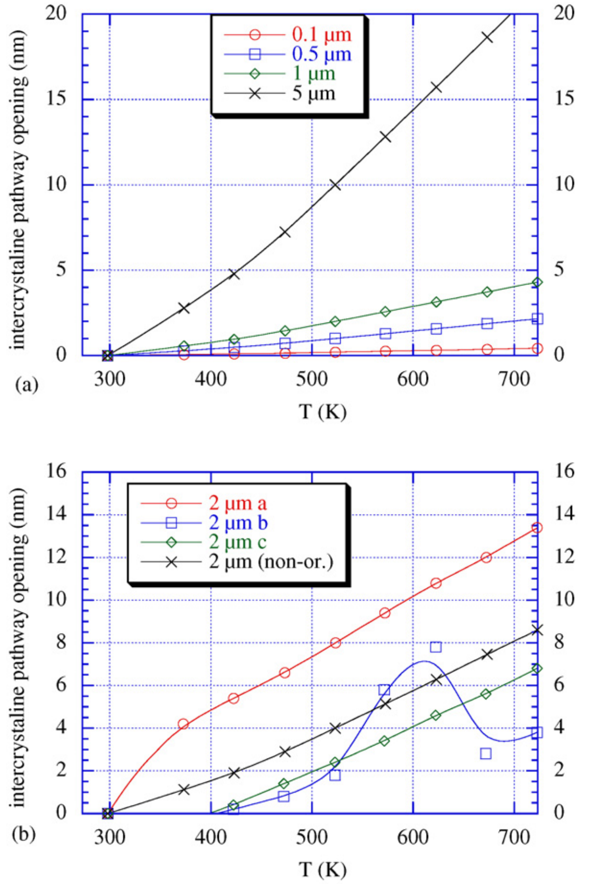

Fig. 7. Intercrystalline pore opening due to the thermal expansion mismatch between support and zeolite crystals in film-like membranes: (a) calculations based on non-oriented crystals, as a function of crystal size; (b) 2 μm crystals oriented along a, b, c and non-oriented (calculated from data of [55]).

On the basis of the above approach, for crystal size ranges commonly shown in the articles dealing with zeolite membranes (0.5–5 μm, see Table 2), intercrystalline pore openings become larger than zeolite pores in the temperature range usually applied for testing gas permeance. This effect is even more pronounced at higher temperatures. For instance, non-oriented 2 μm crystals lead to 6 nm intercrystalline pores at 600 K. At this temperature, such large pores represent about 1.2% of the membrane surface area. In order to estimate the possible contribution of these openings, one can compare to mesoporous membranes. Typical hydrogen permeance values obtained in this group on commercial mesoporous membranes of the same pore size and comparable thickness are close to 10 μmol/m^2/s/Pa, with an open surface of ca. 25% of the geometric area. This suggests a permeance contribution of these openings of about 1 μmol/m^2/s/Pa. This value is larger than typical permeances of film-like zeolite membrane in the range of temperature considered. This approach is likely a succinct and therefore simplified presentation. However, considering the orders of magnitude, it accounts satisfactorily for the permeance increase at higher temperature observed through film-like membranes.

In this phenomenon crystal size matters, but one can imagine that grain size could also, as crystals are generally intergrown, leading to larger units than a single crystal [57]. Then the grain including several crystals would keep in a single part, thus accumulating the thermal contraction effect of all crystals it contains. This secondary issue of crystal/grain size is most likely linked, on top the intergrowth effect, to the zeolite/support adhesion and therefore difficult to estimate. In any case, the values presented in Fig. 7 should then be increased. Similar phenomena, but at a larger scale, together with template removal influence on crystal size, could originate the crack formation in zeolite top-layers during the calcination step [58].

Results shown in Fig. 7 can be discussed together with experimental thermal measurements on membranes published by Gualtieri et al. [23]. This group showed, using an X-ray high resolution technique that, upon heating, the film-like membrane MFI crystals follow the contraction also observed in the MFI powder, which can be translated into gap openings as indicated in Fig. 7. However, on a sample prepared in a way that part of the crystals were embedded into the alumina matrix, they observe a different thermal behaviour. In this case, the reported MFI cell volume was constant, suggesting that the embedded crystals do not follow the natural thermal contraction. In fact, this constant value is an average, corresponding to (i) film crystals and (ii) crystals embedded in the support pores. Considering that the film crystal size follows the normal thermal contraction behaviour, one could suppose that the embedded MFI actually follows the thermal expansion of the support.

This situation (ii) is close to the nanocomposite architecture described in this work, where single zeolite crystals are grown inside the support pores [38]. Accordingly, it can be reasonably assumed that the present membranes are not submitted to the intercrystalline pore opening behaviour. This is in agreement with the absence of high temperature flux increase observed in Figs. 2–5.

The reason for this particular behaviour can be discussed on the basis of the MFI-alumina nanocomposite composition. The support porosity being close to 25%, the weight percent of zeolite in the material is close to 12%. Moreover, as observed in our previous work, the zeolite crystal is constraint by the surrounding alumina grains, with which its whole surface is closely linked (much more than in film-like membranes). Therefore, it can be thought that the support rules the thermal behaviour of the composite material.

Finally, the absence of intercrystalline pore opening is consistent with the modelling of single gas permeations based only on the Maxwell–Stefan approach, which takes into account exclusively intracrystalline transport [39,40].

As a conclusion for this section, the nanocomposite MFI-alumina membrane offers a different thermal behaviour for gas permeance. This characteristic may have important consequences on the gas separation properties of this type of membrane.

4.3. *Consequences in gas separation*

Comparing the hydrogen/*n*-butane separation data presented in Fig. 4 with literature is not straightforward, as very few papers present similar experiments on such a wide temperature range. However, Kapteijn's group have presented a temperature variation showing a continuous hydrogen flux increase over 400 K [15], whereas Fig. 4 shows a maximum at 570 K without any flux increase further on. This is in agreement with the idea that the film-like membrane opens intercrystalline pores that contribute increasingly to the transport above a certain temperature. Similar considerations can explain *n*-butane flux variations. As in film-structured membranes, intercrystalline pathways opening with temperature can reach sizes larger that the zeolitic pore, one may expect a drop of gas separation factor, when compared to nanocomposites.

This difference between film-like samples and our nanocomposite membranes has also been observed for ethanol/oxygen separation [59]. These results showed a higher selectivity for ethanol through nanocomposite material at increased temperatures.

As for xylene separation, the comparison of this work with literature data is easier. Indeed, as this operation draws more interest, numerous results can be found, due to potential direct industrial applications. Fig. 5 shows that nanocomposite MFI-alumina membranes offer a fully permselective behaviour in favour of *para*-xylene, over the complete 400–700 K temperature range, which covers the widest ones published. A flux maximum is observed at 450 K, in good keeping with the majority of literature data presented in Table 3. Nevertheless, most of the works dealing with temperatures high enough also report a flux inflexion generally between 460 and 570 K, leading to a permeance increase with temperature. Moreover, it has to be noted that this increase usually comes with a drop in permselectivity. This trend reinforces the idea of thermal pore opening in film-like zeolite membranes. However, as mentioned in Fig. 7, the larger the crystal size, the larger the effect. This could be the reason why in [30], where the membrane crystal size is very small (<0.2 μm), the xylene flux keeps on a decreasing trend, at least up to 650 K (range limit). In this case, the intercrystalline pore opening would be limited to about 0.5 nm at this temperature, which happens to be equivalent to the MFI pore size. On the other hand, Tarditi et al. [28], using membranes with very large crystals (≈15 μm), observe an increase in flux for all isomers starting at temperatures as low as 420 K. Contrarily, with nanocomposite membranes (Fig. 5) the *para*-xylene flux decreases regularly, and the membrane maintains an apparent infinite selectivity over the whole temperature range.

5. Conclusion

Contrarily to film-structured zeolite membranes, nanocomposites do not show intercrystalline pore opening when increasing temperature. As a consequence, gas transport and separation, using nanocomposite MFI-alumina membranes are controlled, whatever the temperature, by the intrinsic properties (pore size, adsorption characteristics) of the zeolite material.

The present material shows a very low Si/Al ratio. This is an interesting point, because with such a very large number of acidic sites, one can expect a wide range of possibilities for membrane modifications. Moreover, this low ratio is reported to make the synthesis of defect-free membranes difficult [46], which is not the case here.

From a more general point of view, this nanocomposite membrane architecture could lead to a new approach to solve the problem of thermal expansion mismatch between support and separative materials, and therefore limit the effect of grain boundary opening. This paper underlines these thermal effects on MFI, lacking data on other systems, but one could expect similar conclusions for other zeolites. This may open innovative routes for the synthesis of membranes relying on other types of zeolites or nanostructured separative materials. Most of the zeolite membranes reported in literature for gas separation applications are based on the MFI structure, very few use other zeolite types. This is likely due to the difficulty to generate defect-free films made of zeolite crystals other than MFI. Non gas-tight grain boundaries, intercrystalline pore openings during template removal, beside thermal expansion mismatch with the support, are parameters that may originate defects. They could be suppressed or at least limited using a pore-plugging approach. As a matter of fact, in a nanocomposite architecture, mainly single zeolite crystals, strongly connected to the support, are present in the pores of the host material and form the separative layer.

Acknowledgements

S.M. and J.-A.D. kindly acknowledge Pr. George R. Gavalas, of the California Institute of Technology, for his encouraging discussions on the aspects of thermal behaviour of composite materials, at the occasion of the IZMM conference in Breckenridge.

References

[1] A.S.T. Chiang, K. Chao, Membranes and films of zeolite and zeolite-like materials, J. Phys. Chem. Solids 62 (2001) 1899–1910.

[2] J. Coronas, J. Santamaría, Separations using zeolite membranes, Sep. Purif. Methods 28 (1999) 127–177.

[3] A. Julbe, Zeolite membranes—a short overview, Stud. Surf. Sci. Catal. 157 (2005) 135–160.

[4] Y.S. Lin, Microporous and dense inorganic membranes: current status and prospective, Sep. Purif. Technol. 25 (2001) 39–55.

[5] Y.S. Lin, I. Kumakiri, B.N. Nair, H. Alsyouri, Microporous inorganic membranes, Sep. Purif. Methods 32 (2002) 229–379.

[6] E.E. McLeary, J.C. Jansen, F. Kapteijn, Zeolite based films, membranes and membrane reactors: progress and prospects, Micropor. Mesopor. Mater. 90 (2006) 198–220.

[7] H. Verweij, Ceramic membranes: morphology and transport, J. Mater. Sci. 38 (2003) 4677–4695.

[8] M. Noack, P. Kölsch, R. Schäfer, P. Toussaint, J. Caro, Molecular sieve membranes for industrial application: problems, progress, solutions, Chem. Eng. Technol. 25 (2002) 221–230.

[9] M. Tsapatsis, G.R. Gavalas, Synthesis of porous inorganic membranes, MRS Bull. 24 (1999) 30–35.

[10] Z. Lai, G. Bonilla, I. Diaz, J.G. Nery, K. Sujaoti, M.A. Amat, E. Kokkoli, O. Terasak, R.W. Thompson, M. Tsapatsis, D.G. Vlachos, Microstructural optimization of a zeolite membrane for organic vapor separation, Science 300 (2003) 456–460.

[11] R.D. Noble, J.L. Falconer, Silicalite-1 zeolite composite membranes, Catal. Today 25 (1995) 209–212.

[12] F. Kapteijn, J.M. Van de Graaf, J.A. Moulijn, One-component permeation maximum: diagnostic tool for silicalite-1 membranes? AIChE J. 46 (2000) 1096–1100.

[13] Z.A.E.P. Vroon, K. Keizer, M.J. Gilde, H. Verweij, A.J. Burggraaf, Transport properties of alkanes through ceramic thin zeolite MFI membranes, J. Membr. Sci. 113 (1996) 293–300.

[14] C. Bai, M. Jia, J.L. Falconer, R.D. Noble, Preparation and separation properties of silicalite composite membranes, J. Membr. Sci. 105 (1995) 79–87.

[15] F. Kapteijn, W.J.W. Bakker, J.V. van de Graaf, G. Zheng, J. Poppe, J.A. Moulijn, Permeation behaviour of a silicate-1 membrane, Catal. Today 25 (1995) 213–218.

[16] M. Tsapatsis, G. Xomeritakis, Zeolite membranes, Cattech 3 (2000) 148–163.

[17] E.R. Geus, H. van Bekkum, Calcination of large MFI-type single crystals. Part 2. Crack formation and thermomechanical properties in view of the preparation of zeolite membranes, Zeolites 15 (1995) 333–341.

[18] E.R. Geus, H. van Bekkum, W.J.W. Bakker, J.A. Moulijn, High-temperature stainless steel supported zeolite (MFI) membranes: preparation, module construction, and permeation experiments, Micropor. Mater. 1 (1993) 131–147, doi:10.1016/0927-6513(93)80019-Q.

[19] M.P. Bernal, J. Coronas, M. Menendez, J. Santamaría, Characterization of zeolite membranes by temperature programmed permeation and step desorption, J. Membr. Sci. 195 (2001) 125–138.

[20] J. Coronas, J.L. Falconer, R.D. Noble, Characterization permeation properties pf ZSM-5 tubular membranes, AIChE J. 43 (1997) 1797–1812.

[21] J. Hedlund, J. Sterte, M. Anthonis, A. Bons, B. Carstensen, N. Corcoran, D. Cox, H. Deckman, W.D. Gijnst, P. Moor, F. Lai, J. McHenry, W. Mortier, J. Reinoso, J. Peters, High-flux MFI membranes, Micropor. Mesopor. Mater. 52 (2002) 179–189.

[22] S. Gopalakrishnan, T. Yamaguchi, S. Nakao, Permeation properties of templated and template-free ZSM-5 membranes, J. Membr. Sci. 274 (2006) 102–107.

[23] L.M. Gualtieri, A.F. Gualtieri, J. Hedlund, F. Jareman, J. Sterte, M. Dapiaggi, Accurate measurement of the thermal expansion of MFI zeolite membranes by in situ HTXRPD, Stud. Surf. Sci. Catal. 154A (2004) 703–709.

[24] Y. Sasaki, W. Shimizu, Y. Ando, H. Saka, Microstructure analysis with TEM for zeolite layer formed in pore of porous alumina substrate, Micropor. Mesopor. Mater. 40 (2000) 63–71.

[25] W.J.W. Bakker, F. Kapteijn, J. Poppe, J.A. Moulijn, Permeation characteristics of a metal-supported silicalite-1 zeolite membrane, J. Membr. Sci. 117 (1996) 57–78, doi:10.1016/0376-7388(96)00035-X.

[26] W.J.W. Bakker, L.J.P. Van Den Broeke, F. Kapteijn, J.A. Moulijn, Temperature dependence of one-component permeation through a silicalite-1 membrane, AIChE J. 43 (1997) 2203–2214.

[27] G. Li, E. Kikuchi, M. Matsukata, ZSM-5 zeolite membranes prepared from a clear template-free solution, Micropor. Mesopor. Mater. 60 (2003) 225–235.

[28] A.M. Tarditi, S. Irusta, E.A. Lombardo, Xylene isomerization in a membrane reactor: Part I: The synthesis of MFI membranes for the p-xylene separation, Chem. Eng. J. 122 (2006) 167–174, doi:10.1016/j.cej.2006.06.009.

[29] A.J. Burggraaf, Single gas permeation of thin zeolite (MFI) membranes: theory and analysis of experimental observations, J. Membr. Sci. 155 (1999) 45–65.

[30] J. Hedlund, F. Jareman, A. Bons, M. Anthonis, A masking technique for high quality MFI membranes, J. Membr. Sci. 222 (2003) 163–179.

[31] D. Uzio, J. Peureux, A. Giroir-Fendler, J.A. Dalmon, J.D.F. Ramsay, Formation and pore structure of zeolite membranes, Stud. Surf. Sci. Catal. 87 (1994) 411–418.

[32] A. Giroir-Fendler, J. Peureux, H. Mozzanega, J.A. Dalmon, Characterisation of a zeolite membrane for catalytic membrane reactor application, Stud. Surf. Sci. Catal. 101A (1996) 127–136.

[33] P. Ciavarella, H. Moueddeb, S. Miachon, K. Fiatty, J.A. Dalmon, Experimental study and numerical simulation of hydrogen/isobutane permeation and separation using MFI-zeolite membrane reactor, Catal. Today 56 (2000) 253–264, doi:10.1016/S0920-5861(99)00283-7.

[34] O. Pachtová, I. Kumakiri, M. Kocirik, S. Miachon, J.A. Dalmon, Dynamic desorption of adsorbing species under cross membrane pressure difference: a new defect characterisation approach in zeolite membranes, J. Membr. Sci. 226 (2003) 101–110, doi:10.1016/j.memsci.2003.07.017.

[35] D. Casanave, A. Giroir-Fendler, J. Sanchez, R. Loutaty, J.A. Dalmon, Control of transport properties with a microporous membrane reactor to enhance yields in dehydrogenation reactions, Catal. Today 25 (1995) 309–314.

[36] P. Ciavarella, D. Casanave, H. Moueddeb, S. Miachon, K. Fiaty, J.A. Dalmon, Isobutane dehydrogenation in a membrane reactor. Influence of the operating conditions on the performance, Catal. Today 67 (2001) 177–184, doi:10.1016/S0920-5861(01)00311-X.

[37] L. van Dyk, L. Lorenzen, S. Miachon, J.A. Dalmon, Xylene isomerization in an extractor type catalytic membrane reactor, Catal. Today 104 (2005) 274–280, doi:10.1016/j.cattod.2005.03.043.

[38] S. Miachon, E. Landrivon, M. Aouine, Y. Sun, I. Kumakiri, Y. Li, O. Pachtová Prokopová, N. Guilhaume, A. Giroir-Fendler, H. Mozzanega, J.A. Dalmon, Nanocomposite MFI-alumina membranes via pore-plugging synthesis. Preparation and morphological characterisation, J. Membr. Sci. 281 (2006) 228–238, doi:10.1016/j.memsci.2006.03.036.

[39] R. Krishna, R. Baur, Modelling issues in zeolite based separation processes, Sep. Purif. Technol. 33 (2003) 213–254, doi:10.1016/S1383-5866(03)00008-X.

[40] R. Krishna, L.J.P. vand den Broeke, The Maxwell–Stefan description of mass transport across zeolite membranes, Chem. Eng. J. 57 (1995) 155–162.

[41] J.T. Gleaves, G.S. Yablonski, P. Phanawadee, Y. Schuurman, TAP-2: an interrogative kinetics approach, Appl. Catal. A: Gen. 160 (1997) 55–88.

[42] Y. Schuurman, A. Pantazidis, C. Mirodatos, The TAP-2 reactor as an alternative tool for investigating FCC catalysts, Chem. Eng. Sci. 54 (1999) 3619–3625.

[43] W. Zhu, J.M. van de Graaf, L.J.P. van den Broeke, F. Kapteijn, J.A. Moulijn, TEOM: a unique technique for measuring adsorption properties. light alkanes in silicalite-1 industrial & engineering chemistry research, Ind. Eng. Chem. Res. 37 (1998) 1934–1942, doi:10.1021/ie970739q.

[44] H. Jobic, M. Bee, G.J. Kearley, Dynamics of ethane and propane in zeolite ZSM-5 studied by quasi-elastic neutron scattering, Zeolites 12 (1992) 146–151, doi:10.1016/0144-2449(92)90075-Z.

[45] B.S. Kang, G.R. Gavalas, Intrapore synthesis of silicalite membranes at temperatures below 100 °C, Ind. Eng. Chem. Res. 41 (2002) 3145–3150.

[46] M. Noack, P. Kolsch, V. Seefeld, P. Toussaint, G. Georgi, J. Caro, Influence of the Si/Al-ratio on the permeation properties of MFI-membranes, Micropor. Mesopor. Mater. 79 (2005) 329–337, doi:10.1016/j.micromeso.2005.01.004.

[47] H. Takaba, A. Yamamoto, S. Nakao, Modeling of methane permeation through a defective region in MFI-type zeolite membranes, Micropor. Mesopor. Mater. 192 (2006) 82–90, doi:10.1016/j.desal.2005.09.018.

[48] L.T.Y. Au, K.L. Yeung, An investigation of the relationship between microstructure and permeation properties of ZSM-5 membranes, J. Membr. Sci. 194 (2001) 33–55.

[49] J. Dong, Y.S. Lin, M.Z. Hu, R.A. Peascoe, E.A. Paysant, Template-removal-associated microstructural development of porous-ceramic-supported MFI zeolite membranes, Micropor. Mesopor. Mater. 34 (2000) 241–253.

[50] H. Jeong, Z. Lai, M. Tsapatsis, J.C. Hanson, Strain of MFI crystals in membranes: an in situ synchrotron X-ray study, Micropor. Mesopor. Mater. 84 (2005) 332–337, doi:10.1016/j.micromeso.2005.05.043.

[51] O. Pachtová, M. Kocirík, A. Zikánová, B. Bernauer, S. Miachon, J.A. Dalmon, A comparative study of template removal from silicalite-1 crystals in pyrolytic and oxidizing regimes, Micropor. Mesopor. Mater. 55 (2002) 285–296, doi:10.1016/S1387-1811(02)00430-4.

[52] K. Yamahara, K. Okazaki, K. Kawamura, Molecular dynamics studies on thermal behavior of an MH-type zeolite, Catal. Today 23 (1995) 397–402.

[53] S.H. Park, R.W. Große Kunstleve, H. Graetsch, H. Gies, The thermal expansion of the zeolites MFI, AFI, DOH, and MTN in their calcined and as synthesized forms, Stud. Surf. Sci. Catal. 105 (1997) 1989–1994.

[54] B.A. Marinkovic, P.M. Jardim, A. Saavedra, L.Y. Lau, C. Baehtz, R.R. de Avillez, F. Rizzo, Negative thermal expansion in hydrated HZSM-5 orthorhombic zeolite, Micropor. Mesopor. Mater. 71 (2004) 117–124.

[55] D.S. Bhange, V. Ramaswamy, Negative thermal expansion in silicalite-1 and zirconium silicalite-1 having MFI structure, Mater. Res. Bull. 41 (2006) 1392–1402.

[56] M.C. Dalconi, G. Cruciani, A. Alberti, P. Ciambelli, Overloaded Cu-ZSM-5 upon heating treatment: a time resolved X-ray diffraction study, Micropor. Mesopor. Mater. 94 (2006) 139–147, doi:10.1016/j.micromeso.2006.03.047.

[57] M.A. Snyder, Z. Lai, M. Tsapatsis, D.G. Vlacho, Combining simultaneous reflectance and fluorescence imaging with SEM for conclusive identification of polycrystalline features of MFI membranes, Micropor. Mesopor. Mater. 76 (2004) 29–33.

[58] M. Lassinantti Gualtieri, C. Andersson, F. Jareman, J. Hedlund, A.F. Gualtieri, M. Leoni, C. Meneghini, Crack formation in [alpha]-alumina supported MFI zeolite membranes studied by in situ high temperature synchrotron powder diffraction, J. Membr. Sci. 290 (2007) 95–104, doi:10.1016/j.memsci.2006.12.018.

[59] E. Piera, A. Giroir-Fendler, J.A. Dalmon, H. Moueddeb, J. Coronas, M. Menendez, J. Santamaria, Separation of alcohols and alcohols/O_2 mixtures using zeolite MFI membranes, J. Membr. Sci. 142 (1998) 97–109.

[60] C.L. Flanders, V.A. Tuan, R.D. Noble, J.L. Falconer, Separation of C6 isomers by vapor permeation and pervaporation through ZSM-5 membranes, J. Membr. Sci. 176 (2000) 43–53.

[61] K. Aoki, V.A. Tuan, J.L. Falconer, R.D. Noble, Gas permeation properties of ion-exchanged ZSM-5 zeolite membranes, Micropor. Mesopor. Mater. 39 (2000) 485–492, doi:10.1016/S1387-1811(00)00224-9.

[62] J. Hedlund, M. Noack, P. Kolsch, D. Creaser, J. Caro, J. Sterte, ZSM-5 membranes synthesized without organic templates using a seeding technique, J. Membr. Sci. 159 (1999) 263.

[63] M.P. Bernal, E. Piera, J. Coronas, M. Menéndez, J. Santamaría, Mordenite and ZSM-5 hydrophilic tubular membranes for the separation of gas phase mixtures, Catal. Today 56 (2000) 221–227.

[64] A. Julbe, D. Farrusseng, J.C. Jalibert, C. Mirodatos, C. Guizard, Characteristics and performance in the oxidative dehydrogenation of propane of MFI and V-MFI zeolite membranes, Catal. Today 56 (2000) 199–209.

[65] C.J. Gump, V.A. Tuan, R.D. Noble, J.L. Falconer, Aromatic permeation through crystalline molecular sieve membrane, Ind. Eng. Chem. Res. 40 (2001) 565–577.

[66] G. Xomeritakis, Z. Lai, M. Tsapatsis, Separation of xylene isomer vapors with oriented MFI membranes made by seeded growth industrial & engineering chemistry research, Ind. Eng. Chem. Res. 40 (2001) 544–552, doi:10.1021/ie000613k.

[67] Z. Lai, M. Tsapatsis, Gas and organic vapor permeation through b-oriented MFI membranes, Ind. Eng. Chem. Res. 43 (2004).

[68] X. Gu, J. Dong, T.M. Nenoff, D.E. Ozokwelu, Separation of *p*-xylene from multicomponent vapor mixtures using tubular MFI zeolite membranes, J. Membr. Sci. 280 (2006) 624–633.